Interferometry-Integrated Noise-Immune Quantum Memory

Zhifei Yu,[1] Zeliang Wu,[1] Xuejie Li,[1] Xiaotian Feng,[1] Wenfeng Huang,[1] Keye Zhang,[1] Chun-Hua Yuan,[1,*] Weiping Zhang,[2,3,4,5,†] and L. Q. Chen[1,3,‡]

[1]*State Key Laboratory of Precision Spectroscopy, School of Physics and Electronic Science, East China Normal University, Shanghai 200062, China*
[2]*School of Physics and Astronomy, and Tsung-Dao Lee Institute, Shanghai Jiao Tong University, Shanghai 200240, China*
[3]*Shanghai Branch, Hefei National Laboratory, Shanghai 201315, China*
[4]*Collaborative Innovation Center of Extreme Optics, Shanxi University, Taiyuan, Shanxi 030006, China*
[5]*Shanghai Research center for Quantum Science, Shanghai 201315, China*

(Received 23 April 2023; accepted 18 September 2023; published 12 October 2023)

A quantum memory with the performances of low noise, high efficiency, and high bandwidth is of crucial importance for developing practical quantum information technologies. However, the excess noises generated during the highly efficient processing of quantum information inevitably destroy quantum state. Here, we present a quantum memory with built-in excess-noise eraser by integrating a photon-correlated quantum interferometry in quantum memory, where the memory efficiency can be enhanced and the excess noises can be suppressed to the vacuum level via destructive interference. This quantum memory is demonstrated in a rubidium vapor cell with a 10-ns-long photonics signal. We observe ∼80% noise suppression, the write-in efficiency enhancement from 87% to 96.2% without and with interferometry, and the corresponding memory efficiency excluding the noises from 70% to 77%. The fidelity is 93.7% at the single-photon level, significantly exceeding the no-cloning limit. Such interferometry-integrated quantum memory, the first expansion of quantum interference techniques to quantum information processing, simultaneously enables low noise, high bandwidth, high efficiency, and easy operation.

DOI: 10.1103/PhysRevLett.131.150804

Introduction.—Quantum communication and quantum computing (QCQC) have attracted significant attention since the early 1980s due to the promise for absolute security implications [1–3]. A number of QCQC protocols, such as eavesdropping in quantum cryptography [4,5], quantum repeaters [6–10], and linear optics quantum computing [11–13], are implemented based on atomic quantum memory where quantum information transmitting or mapping between optical systems and atomic systems.

In the past decades, various atomic memory approaches have been developed, including EIT [14–16], Raman process [15,17,18], GEM [19,20], Faraday [21], etc. A common characteristic of these approaches is the requirement of strong driving lights to couple atoms and optical signals. To achieve a perfect quantum memory, quantum characteristics of information are required to be perfectly preserved during the atom-light coupling. However, the strong driving lights inevitably bring excess noises via nonlinear processes to reduce or even destroy the quantum information [22–24]. How to eliminate the excess noise from the nonlinear processes is the core problem in QCQC. Previous strategies are focused on preparing the medium into a quantum system such as BEC [25,26], or reducing the strength of nonlinear coupling by smaller coupling coefficient [27–31]. But such methods require complex technologies to prepare and control quantum systems or sacrifice some properties of quantum information. The presence of nonlinear noises during the processing of quantum information memory remains as the long-standing challenge so far.

Here we develop a counteraction strategy by applying a noise eraser after the memorizer [Fig. 1(a)]. The eraser can suppress the excess noises generated from memory to the vacuum level via nonlinear quantum interference without degrading any memory performance. In experiment, quantum memory and the noise eraser are implemented in a ^{87}Rb atomic vapor cell as shown in Fig. 1(b), and the experimental detail is described in [32]. The input signal $\varepsilon_{\mathrm{in}}$ and strong driving W/R pulses are arranged to pass the atoms twice in the forward and then backward directions, where $\varepsilon_{\mathrm{in}}$ is a 10-ns-long pulse at the single-photon level. A phase shift $\Delta\phi$ is applied on the W/R field in the backward direction via PZT. We call the memory process where the optical fields are only in the forward direction as single-pass memory, that in forward and backward directions as two-pass memory. The single-pass memory is the most commonly used one in reported demonstrations [14–20]. While in current two-pass memory, memory efficiency can be enhanced and the excess noises can be suppressed by destructive interference in the backward direction. Below, we will analyze and demonstrate two-pass memory compared with the single-pass one.

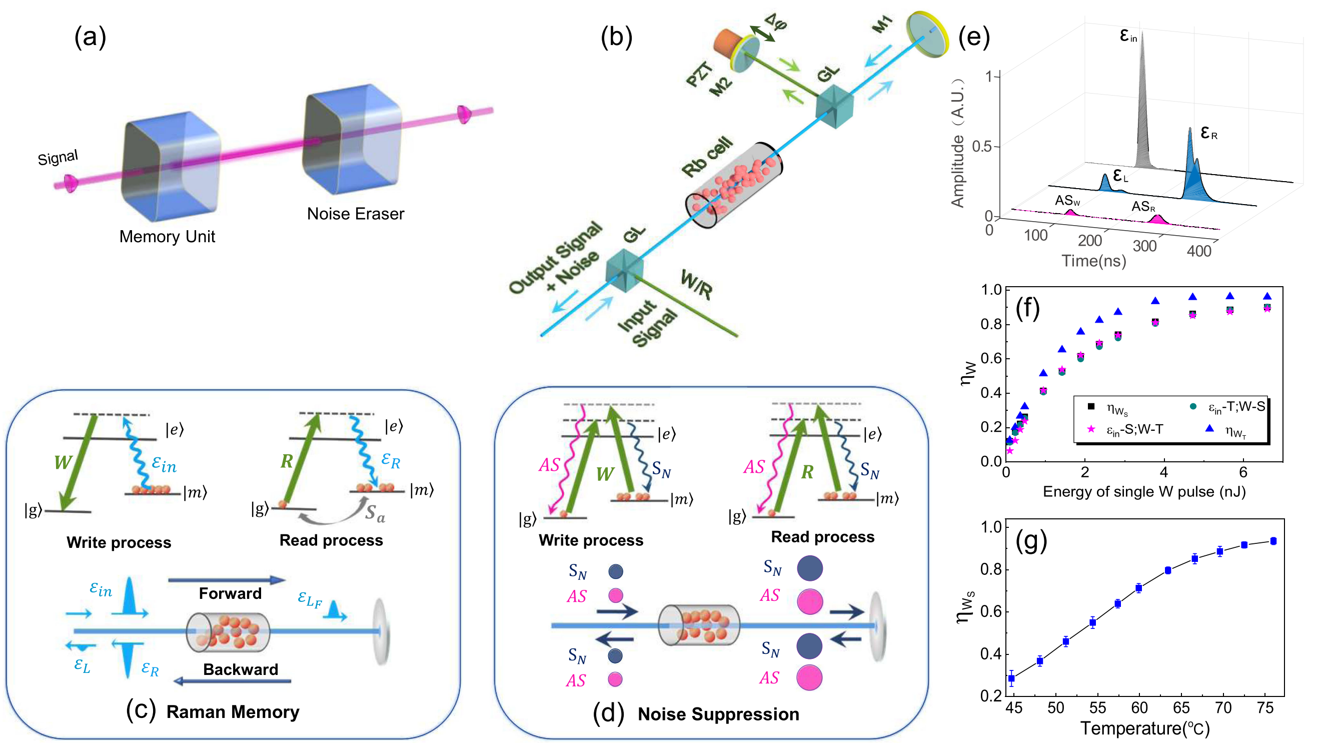

FIG. 1. Noise-immune quantum memory. (a) Quantum memory unit and noise eraser to reduce the noises. (b) Experimental setup. The memory and noise eraser are operated in an ^{87}Rb atomic vapor cell. All optical fields interact with atoms to realize memory in forward direction and then to further memory and suppress noises in backward direction. Glan polarizer (GL); reflected mirror (M); Piezoelectric ceramics (PZT); $\Delta\phi$: phase shift. (c) Two-pass quantum memory. $|g\rangle$: $|5^2S_{1/2}, F=1\rangle$; $|m\rangle$: $|5^2S_{1/2}, F=2\rangle$; $|e\rangle$: $|5^2P_{1/2}, F=2\rangle$; write pulse (W); read pulse (R); $\varepsilon_{\rm in}$: input signal; ε_{L_F}: leaked signal in forward direction; ε_R: the final retrieved signal; ε_L: final leaked signal. (d) Noise suppression by quantum interference. Anti-Stokes (AS); S_N: Stokes noise. The initial S_N and AS vacuum fields, denoted by the blue and purple discs, are amplified as excess noises superposed upon quantum signal after the interaction in forward direction. Then, all optical fields are reflected back and interact with atom in backward direction, where the S_N and AS noises are suppressed back to vacuum fields via destructive interference. The frequency and spatial mode of S_N are the same as the signals $\varepsilon_L/\varepsilon_R$. (e) Single pulse shapes of all signals and noises in single-pass memory. AS_W/AS_R: the AS noise in the write or read process. (f) Write-in efficiency as a function of the energy of a single W pulse. The square curve: single-pass memory η_{W_S}; triangle: the two-pass memory η_{W_T}; circle ($\varepsilon_{\rm in}$-T; W-S): $\varepsilon_{\rm in}$ passes twice but the W pulse only passes once in the forward direction. star ($\varepsilon_{\rm in}$-S; W-T): W passes twice but $\varepsilon_{\rm in}$ only passes once in the forward direction. (g) Write-in efficiency in single-pass memory as a function of the atomic temperature.

Figure 1(c) shows two-pass memory. In the write-in process, the strong W field in the forward direction drives the atoms to coherently absorb part of $\varepsilon_{\rm in}$ as the atomic excitation with efficiency η_{W_F} and then, in the backward direction, drives the atoms to absorb the rest signal ε_{L_F} further with efficiency η_{W_B}. In the read process, the atomic excitations in forward and backward write processes, S_{a_F} and S_{a_B}, are converted to ε_R by the R pulses in respective directions with efficiencies $\eta_{R_F} \sim \eta_{R_B} \sim \eta_R$. S_{a_F} and S_{a_B} have different wave vectors, resulting in that the write and read processes in backward direction are independent with those in the forward direction due to the phase mismatching. And more importantly, the phase shift $\Delta\phi$ on backward W and R fields has no effect on ε_R due to the opposed phase response in the interaction Hamiltonian of the write and read processes [32]. Therefore, the memory efficiency of the two-pass scheme η_{M_T} is contributed by the memories in both the forward and backward directions, $\eta_{M_T} = \eta_{W_F}\eta_R + (1-\eta_{W_F})\eta_{W_B}\eta_R$. Obviously, η_{M_T} is larger than the efficiency of single-pass memory, that is, $\eta_{M_S} = \eta_{W_F}\eta_R$. This is one of advantages of the current memory scheme.

However, the memory process is simultaneously accompanied with nonlinear four-wave-mixing (FWM) process [Fig. 1(d)] with Hamitonian $\hat{H}_{\rm NL} = i\hbar\bar{\xi}_{\rm NL}\hat{\varepsilon}^{\dagger}_{S_N}\hat{\varepsilon}^{\dagger}_{AS} + {\rm H.c.}$ [33]. In single-pass memory, the strong driving fields pass the atoms only in the forward direction to write and readout the signals, AS and S_N are simultaneously generated. AS can be filtered out by the optical filters, but S_N with the same modes and frequency with is superposed upon the signals as noises degrading the fidelity. Both memory efficiency and noise intensity increase with the atom-light coupling strength, so the usual noise elimination by decreasing $\bar{\xi}_{\rm NL}$ causes the reduction of memory efficiency.

In current two-pass memory, mirrors are added to reflect all optical fields back into the atoms in backward direction to construct the noise eraser with Hamiltonian $\hat{H}_{\mathrm{NE}} = i\hbar\bar{\varsigma}_{\mathrm{NE}}\hat{\varepsilon}^{\dagger}_{S_N}\hat{\varepsilon}^{\dagger}_{AS} + \mathrm{H.c.}$ A significant characteristic of S_N and AS generated in the forward direction is phase conjugation. When the driving field W, R couples the phase shift $\Delta\phi$ and interact with S_N and AS in atoms by FWM in the backward direction, the intensities of S_N and AS noises in the final output state depend on the phase shift, which is proportional to $(1 + \cos\Delta\phi)$. There will appear the interference of the S_N and AS noises. In this sense, the FWM processes in forward and backward directions act as the wave splitter and wave recombination of the photon-correlation interferometer [34–36]. When $\Delta\phi = \pi$ and $\bar{\xi}_{\mathrm{NL}} = \bar{\varsigma}_{\mathrm{NE}}$, the noise eraser runs quantum destructive effect on the output state, which can eliminate the nonlinear noises AS and S_N to the vacuum level but quantum signal remains [32].

Therefore, in two-pass memory, the memory efficiency can be improved to ∼100% by enhancing coupling strength, by contrast, the noise can be kept at near zero in principle. But in the single-pass memory, the increase in memory efficiency by enhancing coupling strength is always accompanied with the rapid growth of the excess noise whose intensity might even be larger than the memorized signal. Two-pass memory design has an efficiency enhancement effect as well as noise suppression compared with the commonly reported single-pass memory [32]. Below, we will experimentally demonstrate it.

Efficiency enhancement.—We first focus on the effect of efficiency enhancement. Figure 1(e) shows the single pulse shapes of the $\varepsilon_{\mathrm{in}}$, ε_L, ε_R signals and the AS noise in write and read processes (AS_W, AS_R) after etalons in single-pass along the forward direction. The signals ε_L and ε_R include the noises S_N, whose energies are, respectively, equal to AS_W and AS_R. In the write-in process, the energy of AS_W is ∼26% of ε_L. The write-in efficiency η_{W_S} is ∼83% including the S_N noise by 1-$N_{\varepsilon_L}/N_{\varepsilon_{\mathrm{in}}}$, and increases to ∼87% excluding the S_N noise by 1-$(N_{\varepsilon_L} - N_{AS_W})/N_{\varepsilon_{\mathrm{in}}}$. In the read process, AS_R is ∼13% of ε_R. The read efficiency η_{R_S} is ∼97% including the S_N noise by $N_{\varepsilon_R}/(N_{\varepsilon_{\mathrm{in}}}$-$N_{\varepsilon_L})$ and reduces to ∼80% excluding the S_N noise by $(N_{\varepsilon_R}$-$N_{AS_R})/[N_{\varepsilon_{\mathrm{in}}}$-$(N_{\varepsilon_L} - N_{AS_W})]$. Then, the total memory efficiency in single-pass η_{M_S} is 81% and 70.3% in the case of including and excluding S_N in signals, respectively. Obviously, the nonlinear noises have unignorable impact on quantum memory, especially in the read process.

The measured values of η_W excluding S_N increase with the write energy [Fig. 1(f)] and the atomic temperature [Fig. 1(g)] [37]. In Fig. 1(f), the square curve is the write-in efficiency η_{W_S} in single-pass memory, the star and circle curves represent the write-in efficiency when the W and signal $\varepsilon_{\mathrm{in}}$ input in the forward direction but only W or only ε_L is reflected back in the backward direction. The square, star, and circle curves overlap together, showing that strong W-beam has little effect on the signal in the opposite direction due to two-photon detuning between the signal and W in the opposite directions caused by Doppler broadening. The write-in efficiency of the two-pass memory η_{W_T} (triangle curve) is always larger than η_{W_S}, such that η_{W_T} can reach 96.2% but η_{W_S} is just 87% at the write energy of 5.6 nJ, clearly demonstrating the enhancement advantage of current memory. The read efficiencies are the same, 80%, in single- and two-pass memories. The remaining part of atomic excitation is lost mainly due to the atomic decoherence effect, atomic excitation flying out of the R beam [32]. In accordance with the value of η_{W_S} varying with the atomic temperature, as shown in Fig. 1(g), further increases of efficiency need much higher optical depth by increasing the atomic temperature or the power of W/R pulse, which will be accompanied by serious excess noises in the quantum signal [38]. This point is clearly shown in Fig. 2(a), where the AS energy increases with atomic temperature in an exponential shape, indicating that

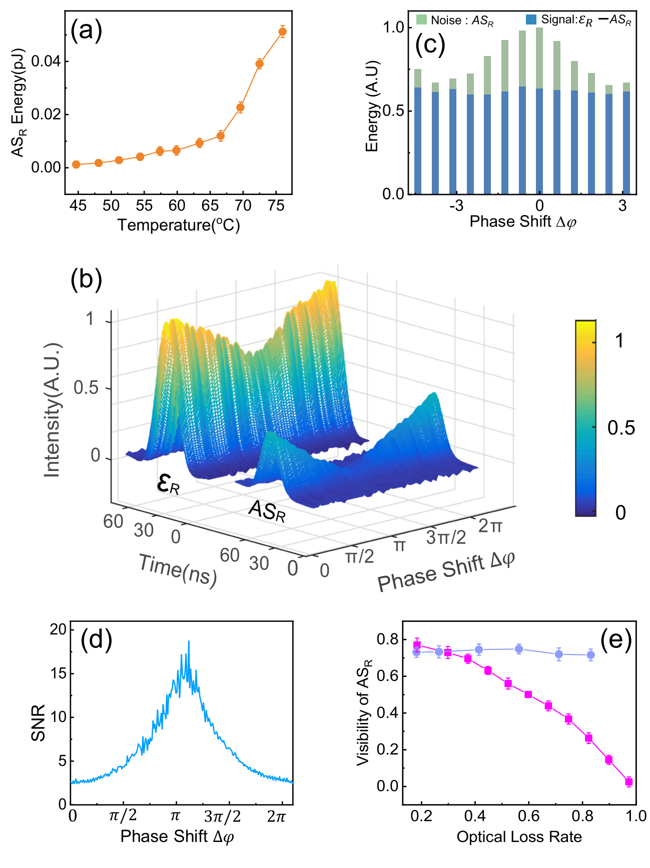

FIG. 2. Noise suppression. (a) The energy of AS_R noise as a function of the atomic temperature in single-pass memory. (b) Single pulse shapes of ε_R and AS_R, (c) the intensities of noise AS_R and signal (ε_R-AS_R), and (d) signal-to-noise ratio (SNR) of ε_R measured by intensity detection as phase shift $\Delta\phi$ scanned from 0 to 2π. (e) Visibility of AS_R as a function of the optical loss rate of W, R (purple square) and AS, S_N (blue dot) in backward direction.

the noises increase much faster than memory efficiency near the saturation region of memory efficiency. Therefore, when performing normal single-pass memory, high efficiency and large noise must be balanced, but it is not required in two-pass memory.

Noise suppression.—We now demonstrate the noise suppression. The S_N and AS noises come from both the amplification and spontaneous processes. In the far off-resonant Raman memory system, spontaneous noise is too small to be detected, while there is significant amplification noise during the memory, especially in the read process (Fig. 1(e)). We focus on ε_R and AS_R. ε_R is consisted of S_N noise and real read signal. To demonstrate the noise suppression of two-pass memory, we measure the intensities of ε_R and AS_R as scanning the phase shift $\Delta\phi$. AS_R and ε_R show interference fringes as $\Delta\phi$ changes [Figs. 2(b) and 2(c)]. The interference visibility of AS_R is ~80%, that is, ~80% AS_R noise can be suppressed at the dark fringe. More importantly, in the corresponding ε_R curve, most S_N noise is also suppressed while the real memory signal is maintained (Fig. 2(c)), clearly demonstrating the significant suppression effect on nonlinear noises of our two-pass memory via quantum interference. Finally, after the noise eraser, the signal-to-noise ratio (SNR), $(\varepsilon_R - AS_R)/AS_R$) is improved seven times [Fig. 2(d)], which can significantly lengthen quantum communication distance and improve the operation times of quantum information [39,40].

In principle, the visibility of AS should be ~100% when $\bar{\xi}_{\rm NL} = \bar{\varsigma}_{\rm NE}$, that is, if there would not be optical loss during the propagation between memory unit and noise eraser, we can achieve near perfect noise suppression [32]. However, in our experiments, there exists optical path loss ~20%, resulting only 80% visibility and noise suppression. In Fig. 2(e), interference visibility decreases with the optical loss rate of the driving field but remains unchanged with the loss of the signal or AS/S_N. The path loss of the driving pulse has significant impact due to $\bar{\xi}_{NL} > \bar{\varsigma}_{NE}$, while the loss in the signal path has little effect on noise suppression but has significant impact on efficiency. Therefore, low-loss optical elements are important to achieve near perfect noise suppression and memory efficiency.

Fidelity.—Next, we analyze the noise performance and give the fidelity. The noise performance of ε_R is analyzed by the variance of quadrature amplitudes of the ε_R pulse using homodyne detection [3,21,41–43]. The variances of quadrature amplitudes at the average photon number of $\varepsilon_{\rm in}$, $\bar{N}_{\varepsilon_{\rm in}} = 30$, are given in Fig. 3. The variance of the coherent pulse $\varepsilon_{\rm in}$ is 0.5 as the reference. The measured variance of ε_R in the single-pass memory (dash-dot line) is 0.7, showing that the intensity fluctuation of ε_R is much larger than that of $\varepsilon_{\rm in}$. Quadrature variance in the two-pass memory changes with phase shift $\Delta\phi$. It is 0.8 at the bright point ($\Delta\phi = 0$), larger than the values of $\varepsilon_{\rm in}$ and ε_R in the single-pass memory. The minimum variance is 0.6 at the destructive interference point ($\Delta\phi = \pi$), larger than $\varepsilon_{\rm in}$ but smaller than ε_R in the single-pass memory. The noise performance of ε_R shows that S_N contributes significant noise fluctuation to the memory signal and can be suppressed in our two-pass memory.

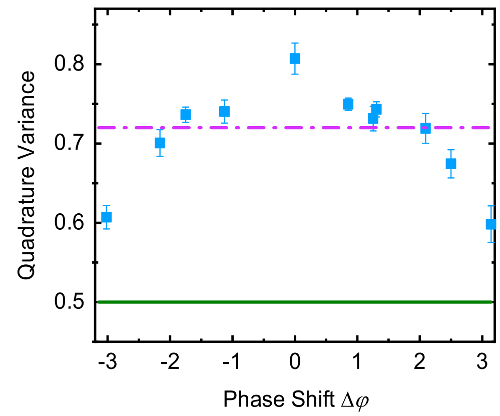

FIG. 3. *Noise performance*. Quadrature variance of ε_R at $\bar{N}_{\varepsilon_{\rm in}} = 30$ as a function of phase shift $\Delta\phi$. Green solid line: $\varepsilon_{\rm in}$; red dash-dot line and blue dot curve are ε_R in single-pass and two-pass memories, respectively.

Table I gives the variance and fidelity values at $\Delta\phi = 0$ and π when $\bar{N}_{\varepsilon_{\rm in}} = 1.25$. As shown in Fig. 2(c), the noise S_N contained in ε_R is smallest at $\Delta\phi = \pi$. That is why $\bar{N}_{\varepsilon_R}$ and the variance of ε_R at $\Delta\phi = \pi$ are both smaller than those at $\Delta\phi = 0$. Furthermore, the fidelity value F at $\Delta\phi = \pi$ is slightly better than at $\Delta\phi = 0$ point. To further investigate the noise impact, we also measure the F_c value, which can remove the influence of noise fluctuation on fidelity. F_c is the fidelity between $\varepsilon_{\rm in}$ and ε_c. ε_c is achieved by attenuating $\varepsilon_{\rm in}$ to same average photon number of ε_R. Therefore, F_c is the best fidelity value under current memory efficiency without the effect of S_N fluctuation. The difference between F_c and F directly reflects the impact of the S_N noise fluctuation on fidelity. Small difference value reflects better noise reduction. The fidelity reduces 3.8% at $\Delta\phi = \pi$, 8.9% at $\Delta\phi = 0$, showing that suppressing the FWM noise has positive effect on preserving quantum state at destructive point. Figure 3 and Table I have clearly shown the noise-erasing advantage of current memory. Finally, $F = 0.937$ at destructive

TABLE I. The noise performance and fidelity. The average photon number in $\varepsilon_{\rm in}$, $\bar{N}_{\varepsilon_{\rm in}} = 1.25$ photon/pulse. $\bar{N}_{\varepsilon_R}$: the average photon number in ε_R; Variance: variance of ε_R; F: the fidelity value between $\varepsilon_{\rm in}$ and ε_R; F_c: the fidelity value between $\varepsilon_{\rm in}$ and ε_c. ε_c is achieved by attenuating $\varepsilon_{\rm in}$ to the average photon number equal to $\bar{N}_{\varepsilon_R}$. ε_R includes real memory signal and S_N noise.

$\Delta\phi$	$\bar{N}_{\varepsilon_R}$	Variance	Fidelity (F)	F_c
0	1.23	0.64	0.907	0.996
π	1.01	0.563	0.937	0.975

interference at $\bar{N}_{\varepsilon_{\rm in}} = 1.25$, significantly exceeding the no-cloning limit [44–47]. Current memory is a quantum memory.

Conclusion.—Two important advantages of current memory, efficiency enhancement, and noise suppression, have been demonstrated via the off-resonant Raman process in the ^{87}Rb vapor cell. In principle, interferometry-integrated quantum memory could be applied to almost all quantum memory systems, including atomic and solid systems based on various light-matter interactions with strong coupling strength, including the current Raman process, EIT, and GEM. Furthermore, spontaneous FWM noise, which is very small in the far off-resonant process but is dominant in near-resonant interactions, could also be suppressed to vacuum level via the destructive interference, in principle. Integration of quantum interference with quantum memory successfully removes the noise obstacle for practical quantum memory, and simultaneously enables low noise, high bandwidth, and high efficiency. Furthermore, current memory is operated in atomic vapor cell plus several mirrors, therefore, it has the advantage of easy operation. Such a pioneering scheme opens the way to extend quantum metrology techniques from precision measurement to quantum information processing.

This work was supported by Innovation Program for Quantum Science and Technology (2021ZD0303200); the National Natural Science Foundation of China (Grants No. 12274132, No. 12234014, No. 11974111, No. 11974116, No. 12374328, No. 11654005, and No. 91536114); Shanghai Municipal Science and Technology Major Project (2019SHZDZX01); Innovation Program of Shanghai Municipal Education Commission (202101070008E00099); W. Z. also acknowledges additional support from the Shanghai Talent Program; Chinese National Youth Talent Support Program; Fundamental Research Funds for the Central Universities; National Key Research and Development Program of China (2016YFA0302001).

Z. Y. and Z. W. contributed equally to this work.

*chyuan@phy.ecnu.edu.cn
†wpz@sjtu.edu.cn
‡lqchen@phy.ecnu.edu.cn

[1] C. H. Bennett and G. Brassard, *Proceedings of the IEEE International Conference on Computers, Systems and Signal Processing* (IEEE, New York, 1984).
[2] Y.-F. Hsiao, P.-J. Tsai, H.-S. Chen, S.-X. Lin, C.-C. Hung, C.-H. Lee, Y.-H. Chen, Y.-F. Chen, I. A. Yu, and Y.-C. Chen, Highly Efficient Coherent Optical Memory Based on Electromagnetically Induced Transparency, Phys. Rev. Lett. **120**, 183602 (2018).
[3] M. Hosseini, G. Campbell, B. M. Sparkes, P. K. Lam, and B. C. Buchler, Unconditional room-temperature quantum memory, Nat. Phys. **7**, 794 (2011).
[4] D. S. Naik, C. G. Peterson, A. G. White, A. J. Berglund, and P. G. Kwiat, Entangled State Quantum Cryptography: Eavesdropping on the Ekert Protocol, Phys. Rev. Lett. **84**, 4733 (2000).
[5] A. K. Ekert, J. G. Rarity, P. R. Tapster, and G. Massimo Palma, Practical Quantum Cryptography Based on Two-Photon Interferometry, Phys. Rev. Lett. **69**, 1293 (1992).
[6] B. Lauritzen, J. Minář, H. de Riedmatten, M. Afzelius, N. Sangouard, C. Simon, and N. Gisin, Telecommunication-Wavelength Solid-State Memory at the Single Photon Level, Phys. Rev. Lett. **104**, 080502 (2010).
[7] C.-W. Chou, J. Laurat, H. Deng, K. S. Choi, H. De Riedmatten, D. Felinto, and H. J. Kimble, Functional quantum nodes for entanglement distribution over scalable quantum networks, Science **316**, 1316 (2007).
[8] N. Sangouard, C. Simon, H. de Riedmatten, and N. Gisin, Quantum repeaters based on atomic ensembles and linear optics, Rev. Mod. Phys. **83**, 33 (2011).
[9] K. Azuma, K. Tamaki, and H.-K. Lo, All-photonic quantum repeaters, Nat. Commun. **6**, 1 (2015).
[10] L.-M. Duan, M. D. Lukin, J. I. Cirac, and P. Zoller, Long-distance quantum communication with atomic ensembles and linear optics, Nature (London) **414**, 413 (2001).
[11] R. Prevedel, P. Walther, F. Tiefenbacher, P. Böhi, R. Kaltenbaek, T. Jennewein, and A. Zeilinger, High-speed linear optics quantum computing using active feed-forward, Nature (London) **445**, 65 (2007).
[12] T. C. Ralph, A. G. White, W. J. Munro, and G. J. Milburn, Simple scheme for efficient linear optics quantum gates, Phys. Rev. A **65**, 012314 (2001).
[13] Y. L. Lim, A. Beige, and L. C. Kwek, Repeat-Until-Success Linear Optics Distributed Quantum Computing, Phys. Rev. Lett. **95**, 030505 (2005).
[14] K. Hammerer, A. S. Sørensen, and E. S. Polzik, Quantum interface between light and atomic ensembles, Rev. Mod. Phys. **82**, 1041 (2010).
[15] M. Lukin, Colloquium: Trapping and manipulating photon states in atomic ensembles, Rev. Mod. Phys. **75**, 457 (2003).
[16] M. D. Lukin, M. Fleischhauer, R. Cote, L. M. Duan, D. Jaksch, J. I. Cirac, and P. Zoller, Dipole Blockade and Quantum Information Processing in Mesoscopic Atomic Ensembles, Phys. Rev. Lett. **87**, 037901 (2001).
[17] J. Nunn, K. Reim, K. C. Lee, V. O. Lorenz, B. J. Sussman, I. A. Walmsley, and D. Jaksch, Multimode Memories in Atomic Ensembles, Phys. Rev. Lett. **101**, 260502 (2008).
[18] D.-S. Ding, *Broad Bandwidth and High Dimensional Quantum Memory Based on Atomic Ensembles* (Springer, New York, 2018), pp. 91–107.
[19] B. M. Sparkes, M. Hosseini, G. Hétet, P. K. Lam, and B. C. Buchler, Ac Stark gradient echo memory in cold atoms, Phys. Rev. A **82**, 043847 (2010).
[20] G. Hétet, J. J. Longdell, M. J. Sellars, P. K. Lam, and B. C. Buchler, Multimodal Properties and Dynamics of Gradient Echo Quantum Memory, Phys. Rev. Lett. **101**, 203601 (2008).

[21] A. I. Lvovsky, B. C. Sanders, and W. Tittel, Optical quantum memory, Nat. Photonics **3**, 706 (2009).
[22] N. Lauk, C. O'Brien, and M. Fleischhauer, Fidelity of photon propagation in electromagnetically induced transparency in the presence of four-wave mixing, Phys. Rev. A **88**, 013823 (2013).
[23] P. Michelberger, T. Champion, M. Sprague, K. Kaczmarek, M. Barbieri, X. Jin, D. England, W. Kolthammer, D. Saunders, J. Nunn *et al.*, Interfacing GHz-bandwidth heralded single photons with a warm vapour raman memory, New J. Phys. **17**, 043006 (2015).
[24] K. F. Reim, P. Michelberger, K. C. Lee, J. Nunn, N. K. Langford, and I. A. Walmsley, Single-Photon-Level Quantum Memory at Room Temperature, Phys. Rev. Lett. **107**, 053603 (2011).
[25] S. Riedl, M. Lettner, C. Vo, S. Baur, G. Rempe, and S. Dürr, Bose-Einstein condensate as a quantum memory for a photonic polarization qubit, Phys. Rev. A **85**, 022318 (2012).
[26] K. R. Patton and U. R. Fischer, Ultrafast Quantum Random Access Memory Utilizing Single Rydberg Atoms in a Bose-Einstein Condensate, Phys. Rev. Lett. **111**, 240504 (2013).
[27] G. Buser, R. Mottola, B. Cotting, J. Wolters, and P. Treutlein, Single-photon storage in a ground-state vapor cell quantum memory, PRX Quantum **3**, 020349 (2022).
[28] D. J. Saunders, J. H. D. Munns, T. F. M. Champion, C. Qiu, K. T. Kaczmarek, E. Poem, P. M. Ledingham, I. A. Walmsley, and J. Nunn, Cavity-Enhanced Room-Temperature Broadband Raman Memory, Phys. Rev. Lett. **116**, 090501 (2016).
[29] S. E. Thomas, T. M. Hird, J. H. D. Munns, B. Brecht, D. J. Saunders, J. Nunn, I. A. Walmsley, and P. M. Ledingham, Raman quantum memory with built-in suppression of four-wave-mixing noise, Phys. Rev. A **100**, 033801 (2019).
[30] I. Vurgaftman and M. Bashkansky, Suppressing four-wave mixing in warm-atomic-vapor quantum memory, Phys. Rev. A **87**, 063836 (2013).
[31] K. Zhang, J. Guo, L. Q. Chen, C. Yuan, Z. Y. Ou, and W. Zhang, Suppression of the four-wave-mixing background noise in a quantum memory retrieval process by channel blocking, Phys. Rev. A **90**, 033823 (2014).
[32] See Supplemental Material at http://link.aps.org/supplemental/10.1103/PhysRevLett.131.150804 for interferometry-integrated noise-immune quantum memory, which includes Refs. [33–36].
[33] R. T. Glasser, U. Vogl, and P. D. Lett, Stimulated Generation of Superluminal Light Pulses via Four-Wave Mixing, Phys. Rev. Lett. **108**, 173902 (2012).
[34] B. Yurke, S. L. McCall, and J. R. Klauder, SU(2) and SU(1,1) interferometers, Phys. Rev. A **33**, 4033 (1986).
[35] W. N. Plick, J. P. Dowling, and G. S. Agarwal, Coherent-light-boosted, sub-shot noise, quantum interferometry, New J. Phys. **12**, 083014 (2010).
[36] F. Hudelist, J. Kong, C. Liu, J. Jing, Z. Ou, and W. Zhang, Quantum metrology with parametric amplifier-based photon correlation interferometers, Nat. Commun. **5**, 3049 (2014).
[37] A. V. Gorshkov, A. André, M. D. Lukin, and A. S. Sørensen, Photon storage in Λ-type optically dense atomic media. ii. free-space model, Phys. Rev. A **76**, 033805 (2007).
[38] S. E. Thomas, J. H. Munns, K. T. Kaczmarek, C. Qiu, B. Brecht, A. Feizpour, P. M. Ledingham, I. A. Walmsley, J. Nunn, and D. J. Saunders, High efficiency Raman memory by suppressing radiation trapping, New J. Phys. **19**, 063034 (2017).
[39] A. Tomaello, C. Bonato, V. Da Deppo, G. Naletto, and P. Villoresi, Link budget and background noise for satellite quantum key distribution, Adv. Space Res. **47**, 802 (2011).
[40] D. Zibar, U. Moura, H.-M. Chin, A. R. Brusin, N. Jain, F. Da Ros, S. Kleis, C. Schaeffer, T. Gehring, U. L. Andersen *et al.*, Advancing classical and quantum communication systems with machine learning, in *Optical Fiber Communication Conference* (OSA, San Diego, 2020), pp. W1K–1.
[41] J. Guo, X. Feng, P. Yang, Z. Yu, L. Chen, C.-H. Yuan, and W. Zhang, High-performance Raman quantum memory with optimal control in room temperature atoms, Nat. Commun. **10**, 148 (2019).
[42] A. MacRae, T. Brannan, R. Achal, and A. I. Lvovsky, Tomography of a High-Purity Narrowband Photon from a Transient Atomic Collective Excitation, Phys. Rev. Lett. **109**, 033601 (2012).
[43] Z. Qin, A. S. Prasad, T. Brannan, A. MacRae, A. Lezama, and A. Lvovsky, Complete temporal characterization of a single photon, Light **4**, e298 (2015).
[44] F. Grosshans and P. Grangier, Quantum cloning and teleportation criteria for continuous quantum variables, Phys. Rev. A **64**, 010301(R) (2001).
[45] G. Hetet, A. Peng, M. T. Johnsson, J. J. Hope, and P. K. Lam, Characterization of electromagnetically-induced-transparency-based continuous-variable quantum memories, Phys. Rev. A **77**, 012323 (2008).
[46] Q. Y. He, M. D. Reid, E. Giacobino, J. Cviklinski, and P. D. Drummond, Dynamical oscillator-cavity model for quantum memories, Phys. Rev. A **79**, 022310 (2009).
[47] B. Julsgaard, J. Sherson, J. I. Cirac, J. Fiurášek, and E. S. Polzik, Experimental demonstration of quantum memory for light, Nature (London) **432**, 482 (2004).